

Trinity College

## Trinity College Digital Repository

---

Faculty Scholarship

---

8-1-2018

### Pseudoelasticity at Large Strains in Au Nanocrystals [post-print]

X. Wendy Gu

*University of California, Berkeley*

Lindsey A. Hanson

*Trinity College Hartford*

Carissa N. Eisler

*Lawrence Berkeley National Laboratory*

Matthew A. Koc

*University of California, Berkeley*

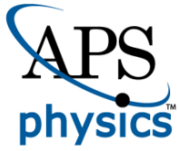
A. Paul Alivisatos

*University of California, Berkeley*

Follow this and additional works at: <https://digitalrepository.trincoll.edu/facpub>

 Part of the [Chemistry Commons](#)

---



# CHORUS

This is the accepted manuscript made available via CHORUS. The article has been published as:

## Pseudoelasticity at Large Strains in Au Nanocrystals

X. Wendy Gu, Lindsey A. Hanson, Carissa N. Eisler, Matthew A. Koc, and A. Paul Alivisatos

Phys. Rev. Lett. **121**, 056102 — Published 1 August 2018

DOI: [10.1103/PhysRevLett.121.056102](https://doi.org/10.1103/PhysRevLett.121.056102)

# Pseudo-Elasticity at Large Strains in Au Nanocrystals

X. Wendy Gu<sup>1,2\*</sup>, Lindsey A. Hanson<sup>1,3\*</sup>, Carissa N. Eisler<sup>4</sup>, Matthew A. Koc<sup>1</sup>, A. Paul Alivisatos<sup>1,4,5,6</sup>

<sup>1</sup>Department of Chemistry, University of California, Berkeley, Berkeley, CA 94720, USA

<sup>2</sup>Department of Mechanical Engineering, Stanford University, Stanford, CA 94305, USA

<sup>3</sup>Department of Chemistry, Trinity College, Hartford, CT 06106, USA

<sup>4</sup>Materials Science Division, Lawrence Berkeley National Laboratory, Berkeley, CA 94720, USA

<sup>5</sup>Department of Materials Science and Engineering, University of California, Berkeley, Berkeley, CA 94720, USA

<sup>6</sup>Kavli Energy NanoScience Institute, University of California, Berkeley and Lawrence Berkeley National Laboratory, Berkeley, CA 94720, USA

\* These authors contributed equally to this work

Corresponding author:

A. Paul Alivisatos

D43 Hildebrand Hall, University of California, Berkeley 94720

510-643-2050

paul.alivisatos@berkeley.edu

Keywords: plasticity, size effects, absorbance, plasmonics, high pressure

1 **Abstract**

2 Pseudoelasticity in metals is typically associated with phase transformations (e.g. shape  
3 memory alloys) but has recently been observed in sub-10 nm Ag nanocrystals that rapidly  
4 recovered their original shape after deformation to large strains. The discovery of  
5 pseudoelasticity in nanoscale metals dramatically changes the current understanding of  
6 the properties of solids at the smallest length scales, and the motion of atoms at surfaces.  
7 Yet, it remains unclear whether pseudoelasticity exists in different metals and nanocrystal  
8 sizes. The challenge of observing deformation at atomistic to nanometer length scales has  
9 prevented a clear mechanistic understanding of nanoscale pseudoelasticity, although  
10 surface diffusion and dislocation-mediated processes have been proposed. We further the  
11 understanding of pseudoelasticity in nanoscale metals by using a diamond anvil cell to  
12 compress colloidal Au nanocrystals under hydrostatic and non-hydrostatic pressure  
13 conditions. Nanocrystal structural changes are measured using optical spectroscopy and  
14 transmission electron microscopy, and modeled using electrodynamic theory. We find  
15 that 3.9 nm Au nanocrystals exhibit pseudoelastic shape recovery after deformation to  
16 large uniaxial strains of up to 20%, which is equivalent to an ellipsoid with an aspect  
17 ratio of 2. Nanocrystal absorbance efficiency does not recover after deformation, which  
18 indicates that crystalline defects may be trapped in the nanocrystals after deformation.

19

20 **Main text**

21 Pseudoelasticity describes the reversible deformation of a material that is strained  
22 past its elastic limit, through a process in which atomic bonds are broken and reformed.  
23 Recently, rapid pseudoelastic recovery from large strains was observed in sub-10 nm Ag

1 nanoparticles inside of a transmission electron microscope (TEM). [1] The surprising  
2 observation of pseudoelasticity in Ag nanoparticles is diametrically opposed to the  
3 classical behavior of metals, in which irreversible plastic deformation occurs at large  
4 strains. This discovery adds to the growing body of evidence that strength, deformation  
5 and defect dynamics in nanoscale solids cannot be extrapolated from the properties of  
6 their bulk counterparts. Pseudoelastic metallic nanostructures should have superior  
7 performance, including shape memory at low temperatures and the ability to rapidly heal  
8 from applied stresses. Pseudoelasticity in metal nanocrystals has been attributed to rapid  
9 surface diffusion, [1,2] but defect mediated processes such as the escape of dislocations  
10 through free surfaces,<sup>13,14</sup> and the reversible passage of twin boundaries [5,6] are other  
11 possible mechanisms. Further insight into this phenomenon requires investigation of  
12 other nanocrystal sizes and metals at realistic temperatures and time scales, which can be  
13 challenging to achieve *in-situ* TEM or through atomistic modeling.

14 Here, 3.9 nm Au nanocrystals are compressed inside of a diamond anvil cell to  
15 determine whether deformation is reversible under volumetric and deviatoric strains. The  
16 outstanding physical properties of Au nanocrystals have enabled their widespread use in  
17 photonics, [7,8] catalysis, [9,10] sensing [11,12] and biomedical therapies. [13,14] The  
18 structural stability of Au nanocrystals is of interest for size and shape control during  
19 synthesis and fabrication, [15,16] and the reliable operation of nanocrystal-based devices.  
20 Pseudoelasticity is expected in 3.9 nm nanocrystals according to the surface diffusion-  
21 based mechanism developed for Ag. [1] It is unclear whether pseudoelasticity will be  
22 observed in Au, which has slower atomic surface diffusion than Ag. [17]

1 Diamond anvil cell compression has previously been used to study elastic  
2 properties and phase transformations in inorganic nanocrystals. [18–23] Nanocrystal  
3 structural changes are monitored *in-situ* using optical absorption spectroscopy.  
4 Absorption spectroscopy reveals the localized surface plasmon resonance of the Au  
5 nanocrystals, which is generated by the resonant oscillation of conduction electrons in  
6 response to light. The energy and intensity of the surface plasmon is highly sensitive to  
7 nanocrystal size and shape, [24–26] and can therefore be used to track deformation under  
8 pressure. The surface plasmon also depends on the density of crystalline defects in the  
9 nanocrystal, [27,28] which is indicative of microstructural changes in the nanocrystals.  
10 We demonstrate the sensitivity of this detection method by using electrostatics theory  
11 to model the optical response to shape and microstructural changes in the Au  
12 nanocrystals. It is found that sub-nanometer changes in nanocrystal aspect ratio lead to  
13 greater than 20 nm shifts in plasmon energy. Results from optical spectroscopy are  
14 corroborated using TEM. Using these techniques, we determine that Au nanocrystals  
15 rapidly recover their original shape after uniaxial deformation to large strains after single  
16 and multicycle loading inside of the diamond anvil cell. We believe that crystalline  
17 defects in the interior of the nanocrystal play a role in the pseudoelastic deformation  
18 based on an irreversible reduction in absorbance efficiency after pressurization.

19 Dodecanethiol-capped Au nanocrystals with diameters of  $3.9 \pm 0.9$  nm were  
20 synthesized using organic-phase air-free techniques (Figure 1A). [29] Nanocrystals were  
21 transferred to the desired pressure medium, and loaded into the diamond anvil cell for  
22 cyclic pressure testing. Ethylcyclohexane was used as a hydrostatic pressure medium, and  
23 toluene was used as a non-hydrostatic pressure medium. [19,30] Nanocrystal solutions

1 were maintained in the dilute limit to ensure that optical changes are not due to particle-  
2 particle coupling. The refractive index of ethylcyclohexane increases by less than 0.006  
3 RIU per GPa, while the refractive index of toluene and dodecanethiol (ligand shell)  
4 increases by 0.02 RIU per GPa (see Supporting Information). Changes in path length and  
5 concentration during pressurization are accounted for by monitoring the cross-sectional  
6 area and height of the diamond anvil cell chamber (see Supporting Information).

7 Figure 1B shows the extinction spectra of the Au nanocrystals under hydrostatic  
8 pressure up to 21 GPa. Extinction is dominated by absorption in nanocrystals that are  
9 much smaller than the wavelength of light, [26] so extinction is referred to as absorbance  
10 from here on out. The absorbance spectra change minimally under hydrostatic pressure.  
11 The plasmon peak wavelength ( $\lambda_{\max}$ ) increases by 5 nm as pressure is increased to 21  
12 GPa (the spectral resolution is 2.7 nm), and returns to the original plasmon wavelength as  
13 pressure is decreased to ambient conditions. The absorbance efficiency at the plasmon  
14 wavelength per volume of solution ( $Q_{\max}$ ) is determined at each pressure. The change in  
15  $Q_{\max}$  from the first to the maximum pressure is within the measurement resolution, as is  
16 the change from the first to the last pressure (ambient pressure). Figure 1C shows the  
17 optical spectra of the Au nanocrystals under non-hydrostatic pressure up to 19 GPa. In  
18 contrast to the hydrostatic case,  $\lambda_{\max}$  undergoes a large redshift as pressure is increased to  
19 19 GPa, and then returns to its original value after the pressure is removed. The shape of  
20 the optical spectrum at the end of the pressure cycle (ambient pressure) is similar to the  
21 initial spectrum, but  $Q_{\max}$  is reduced at the end of the pressure cycle.

22 The changes in plasmon peak wavelength and absorbance efficiency under non-  
23 hydrostatic pressure are quantified in Figure 2 for four experiments. Maximum pressures

1 of 15 to 24 GPa were reached in these experiments, which resulted in a redshift in  $\lambda_{\max}$  of  
2 46 to 68 nm (Figure 2A-D). The average optical shift is 3.2 nm/GPa. Upon removing the  
3 pressure, the final  $\lambda_{\max}$  returned to within 0 to 8 nm of the initial  $\lambda_{\max}$ .  $\lambda_{\max}$  initially shifts  
4 rapidly at pressures below 3 GPa and then shifts more slowly at higher pressures (Figure  
5 2A-D). The corresponding changes in  $Q_{\max}$  are shown in Figure 2E-H. The final  
6 absorbance efficiency is 30% to 60% of the initial absorbance efficiency. The changes in  
7  $Q_{\max}$  with pressure vary across the four experiments (Figure 2E-H). In Figure 2E,  $Q_{\max}$  is  
8 higher at elevated pressures. Figure 2F and H show an initial increase in  $Q_{\max}$  at the first  
9 pressurized data point, and then a decrease in  $Q_{\max}$  below the initial absorbance efficiency  
10 for subsequent pressures. Figure 2G shows an immediate decrease in  $Q_{\max}$  with  
11 pressurization, and a  $Q_{\max}$  that is lower than the initial  $Q_{\max}$  for subsequent pressures. All  
12 experiments show hysteresis in  $Q_{\max}$  between increasing and decreasing pressure.

13 The variation in the optical response across these experiments can be linked to  
14 differences in the magnitude of deviatoric pressure between experiments, and during the  
15 course of an experiment. The deviatoric strain across the sample chamber has been  
16 quantified by measuring the change in cross-sectional area, and distance between the  
17 diamond platens for the experiments in Figure 2, and is observed to vary significantly  
18 between experiments (see Supporting Information). Previous diamond anvil cell  
19 experiments on metallic powders under non-hydrostatic pressures have shown that  
20 uniaxial stress increases linearly with average pressure; [31–33] this is likely to occur  
21 during the experiments presented here as well.

22 Spherical Au nanocrystals will become elongated spheroids under non-hydrostatic  
23 pressure. This change in nanocrystal shape is predicted to lead to a redshift in  $\lambda_{\max}$ , [24–



1 26] which agrees well with our experimental observations. The reversibility of the  
2 observed redshift indicates that the nanocrystals return to their original shape when  
3 pressure is removed, which is quite surprising considering the large pressures involved.  
4 Further evidence of nanocrystal shape recovery is provided by post-deformation TEM  
5 images of the nanocrystals (Figure 3). Nanocrystals were recovered after diamond anvil  
6 cell testing, and dispersed onto a TEM grid. Post-deformation nanocrystals are very  
7 similar in appearance to as-synthesized nanocrystals: nanocrystals are spherical and  
8 contain crystalline domains after deformation (see Supporting Information), and are able  
9 to form close-packed three-dimensional assemblies upon slow drying (Figure 3B).  
10 Ordered nanocrystal assemblies can only form from highly monodisperse  
11 nanocrystals, [34,35] which indicates that a large fraction of nanocrystals are spherical  
12 and reasonably monodisperse after deformation. These results do not explain the  
13 reduction in  $Q_{\max}$  that results from the pressure cycle, which may be due to additional  
14 microstructural changes, like the creation of crystalline defects such as dislocations.

15         The source of the observed changes in  $\lambda_{\max}$  and  $Q_{\max}$  under pressure is  
16 investigated using optical modeling. A finite difference time domain model was used to  
17 calculate absorption of Au nanocrystals of different sizes and shapes, without accounting  
18 for compressional effects (e.g. changes in lattice parameter, electron density or density of  
19 states). The size of the simulated nanocrystal was varied to explore the effect of  
20 volumetric strain on the optical response of Au nanocrystals under hydrostatic pressure  
21 (Figure 4a). Changes in refractive index during compression were accounted for in  
22 simulation. In agreement with the experimental observations, the simulated absorbance  
23 spectra do not change significantly when nanocrystal diameter is changed from 3.9 to 3.5

1 nm. The diameter of the Au nanocrystals is expected to change by this amount in  
2 experiment according to the bulk modulus for a macroscale Au structure [36] although  
3 the bulk modulus may be different for a Au nanocrystal. [20] These results indicate that  
4 compressional effects, such as changes in bound and free electron density under pressure,  
5 are not significant in small Au nanocrystals. The effect of changing electron density is  
6 small because free electrons are delocalized outside of the nanocrystal (electron spillout  
7 effect) in nanocrystals with diameters of less than 10 nm and are not strongly affected by  
8 lattice contraction. [26,37,38] A previous simulation study observed a redshift of more  
9 than 100 nm in 10-100 nm Au nanocrystals under 5% volumetric compression when  
10 electron density effects are prominent. [37]

11 The simulated and experimental spectra for Au nanocrystals under hydrostatic  
12 pressure indicate that a small change in volume has a negligible effect on Au plasmonic  
13 properties. Therefore, the effect of volumetric strain can be omitted in regard to the large  
14 changes in  $\lambda_{\max}$  and  $Q_{\max}$  under non-hydrostatic pressure, although a small amount of  
15 volumetric strain occurs in these tests. The optical spectra of oblate spheroids are  
16 simulated to quantify the effects of deviatoric strain on Au nanocrystals under non-  
17 hydrostatic pressure (Figure 4B). Figure 4b shows the absorbance spectra of spheroidal  
18 Au nanocrystals with aspect ratios (AR) of 1 to 2.7 (AR is defined as the ratio of the  
19 major axis to minor axis of the ellipsoidal cross-section of the spheroid), and volume  
20 equal to a 3.9 nm sphere.  $\lambda_{\max}$  increases from 505 nm to 600 nm when aspect ratio is  
21 increased from 1 to 2.7 (Figure 4C).  $Q_{\max}$  increases to 1.12 a.u. when aspect ratio is  
22 increased to 1.2, due to the changing refractive index environment.  $Q_{\max}$  decreases with  
23 further increases in aspect ratio (Figure 4D). These results support the conclusion that the

1 experimentally observed redshift under non-hydrostatic pressure is due to nanocrystal  
2 shape change.

3 While the initial increase and subsequent decrease in the simulated  $Q_{\max}$  is similar  
4 to experiment (Figure 2E, F, H), the magnitude of the decrease in  $Q_{\max}$  is larger in  
5 experiment than simulation. In particular, the large decrease in the experimental  $Q_{\max}$  that  
6 occurs upon decreasing pressure to ambient conditions does not match the simulated  
7 change in  $Q_{\max}$ , and cannot be attributed to changes in nanocrystal geometry. Previous  
8 experiments show that polycrystalline Au and Ag nanocrystals have lower absorbance  
9 efficiency ( $Q_{\max}$ ) than single crystalline nanocrystals, but similar plasmon wavelength  
10 ( $\lambda_{\max}$ ). [27,28] In contrast, electrodynamic simulations on crystalline defects in Au  
11 nanoshells determined that defects have no influence on optical absorbance, [39] while  
12 atomistic simulations on Ag nanocubes observed a significant redshift and reduction in  
13 absorbance efficiency in sub-3 nm nanocrystals containing planar defects (e.g. partial and  
14 full dislocations). [40] These conflicting reports indicate that further studies are needed to  
15 understand the effect of defects on noble nanocrystal plasmonic properties. The presence  
16 of crystalline defects is modeled in our simulation as an increase in free electron damping  
17 (see Supporting Information). The density of crystalline defects is increased until  
18 equivalent to a Au thin film with a 1.2 nm grain size. [41] This leads to a 10 nm redshift  
19 and a 33% decrease in absorbance efficiency. This result indicates that the experimentally  
20 observed changes in  $\lambda_{\max}$  and  $Q_{\max}$  are due to a combination of shape change and the  
21 emergence of defects in the Au nanocrystals under pressure.

22 Using these simulation results, we estimate that the Au nanocrystals experience  
23 uniaxial strain of up to 14-20% in the non-hydrostatic experiments assuming that the Au

1 nanocrystals become oblate spheroids under pressure with aspect ratios of 1.6 to 2. This  
2 strain far exceeds the elastic limit for bulk Au. Previous diamond anvil cell experiments  
3 on Au and other metals in non-hydrostatic environments show that yield strength  
4 increases by  $\sim 1$  GPa over the pressure range in our experiments. [32,33,42] The uniaxial  
5 pressure in our experiments exceeds the pressure-dependent yield stress for Au such that  
6 plastic deformation (breaking of atomic bonds) is expected to occur in the Au  
7 nanocrystals. The reversible deformation observed in the Au nanocrystals involves a  
8 pseudoelastic transformation in which the Au nanocrystals recover their original shape  
9 after atoms within the nanocrystals lose their original coordinates and connectivity. This  
10 agrees with the recent observation of pseudoelasticity in sub-10nm Ag nanocrystals, [1]  
11 but is the first time this phenomenon has been observed in an ensemble of nanocrystals,  
12 and outside of an electron microscope. Previous diamond anvil cell experiments on  $\sim 40$   
13 nm colloidal Au nanocrystals at dilute concentrations under non-hydrostatic conditions  
14 resulted in irreversible deformation and fracture under pressure. [21,22] Thus,  
15 pseudoelasticity is active on experimental time scales (minutes) only in very small Au  
16 nanocrystals.

17 No dislocations were observed during the pseudoelastic deformation of sub-10 nm  
18 Ag nanocrystals, [1] although there may be dislocations that are invisible at the imaging  
19 conditions, or that move too rapidly to be captured by TEM. In contrast, our optical  
20 measurements and modeling indicate that crystalline defects form in the interior of the  
21 Au nanocrystals during deformation. The mechanism behind the pseudoelasticity in the  
22 Au nanocrystals is investigated by compressing nanocrystal samples over two pressure  
23 cycles to determine the time and history dependence of the optical response. Figure 5A

1 and C correspond to an experiment in which pressure cycle 2 occurred thirty minutes  
2 after the end of cycle 1. The change in  $\lambda_{\max}$  is extremely similar over the two pressure  
3 cycles (Figure 5A). The final  $\lambda_{\max}$  is identical to the initial  $\lambda_{\max}$  after cycle 1, and is  
4 redshifted by 10 nm relative to the initial  $\lambda_{\max}$  after cycle 2. The shape of the  $Q_{\max}$  vs.  
5 pressure curve is similar for the two cycles (Figure 3C), but the initial absorbance  
6 efficiency of cycle 2 is reduced by 0.45 relative to cycle 1. The shape of the  $Q_{\max}$  vs.  
7 pressure curve is similar for the two cycles because the change in strain of the diamond  
8 anvil cell chamber is very similar for the two cycles (see Supporting Information). In the  
9 experiment in Figure 3B and D, cycle 2 occurs 15.5 hours after cycle 1. Interestingly, the  
10 initial  $Q_{\max}$  at the beginning of the second cycle is significantly greater than the final  $Q_{\max}$   
11 of the first cycle (Figure 3D), which indicates that there is recovery of absorbance  
12 efficiency in this time.

13 In the experiments shown in Figure 5, final  $Q_{\max}$  is always lower than the initial  
14  $Q_{\max}$  within one pressure cycle. This indicates that structural deformation accumulates  
15 during the course of the pressure cycle, and can be retained between pressure cycles. The  
16 time dependent changes in  $Q_{\max}$  between pressure cycles presents an intriguing clue as to  
17 the structural changes occurring in the nanocrystals, but require more careful  
18 investigation before conclusions can be made. The post-deformation TEM images of  
19 nanocrystals were taken several days after the diamond anvil cell experiments were  
20 performed (Figure 3). Crystalline defects that were initially present in the nanocrystals  
21 after deformation may have healed before imaging through dislocation-mediated  
22 processes such as escape through free surfaces. [3,4] Direct structural measurements,

1 such as through high-pressure X-ray diffraction, could provide further insights into the  
2 mechanism of pseudoelasticity in Au nanocrystals.

3         In summary, 3.9 nm Au nanocrystals are compressed under hydrostatic and non-  
4 hydrostatic conditions in a diamond anvil cell. Changes in nanocrystal structure under  
5 pressure are monitored using optical absorbance. Nanocrystals under hydrostatic pressure  
6 do not exhibit a change in plasmon wavelength. Nanocrystals under non-hydrostatic  
7 pressure exhibit a reversible redshift of the plasmon wavelength of up to 68 nm over ~20  
8 GPa. The absorbance efficiency is reduced to 30-60% of its original value after the non-  
9 hydrostatic pressure cycle. Optical modeling was performed to correlate changes in  
10 absorbance to strain and lattice disorder in the nanocrystals. The results of this model  
11 indicate that the nanocrystals deform up to ~20% strain (equivalent to an aspect ratio of  
12 2) under non-hydrostatic pressure, yet are able to recover their original spherical shape.  
13 Post-compression TEM images demonstrate that the nanocrystals return to their original  
14 shape after the pressure cycle. The Au nanocrystals exhibit room temperature  
15 pseudoelastic shape recovery at large strains, which differs completely from bulk scale  
16 behavior. A reduction in nanocrystal absorbance efficiency is related to increased free  
17 electron scattering due to the presence of crystalline defects. This indicates that the non-  
18 hydrostatic deformation of Au nanocrystals likely leads to an increase in the number of  
19 defects such as dislocations in the nanocrystals.

20         Our discovery of pseudoelasticity in small Au nanocrystals implies that the  
21 metallic nanostructures used in nanoscale machines, devices and patterned surfaces may  
22 demonstrate rapid self-healing and resilience against external stresses and strains. The  
23 relevance of these findings extends beyond nanofabrication and crystal growth. Au

1 nanocrystals could be used as nanoscale strain gauges that can differentiate between  
2 volumetric and deviatoric strains with a reversible, pressure-dependent optical readout  
3 that has better sensitivity than existing nanocrystal sensors. [19,23,43–45] These  
4 attributes of Au nanocrystals could be used to measure biological forces, which are of  
5 great importance in isolated and collective cell behavior. Our results also present the  
6 possibility of pseudoelastic deformation in nano-precipitates in bulk metallic alloys. It  
7 remains to be seen whether pseudoelasticity is universal across different nanoscale  
8 metals, and when embedded in a variety of matrices.

9  
10

1

## 2 **Acknowledgements**

3 We gratefully acknowledge financial support from the U.S. Department of Energy, Office  
4 of Science, Office of Basic Energy Sciences, Materials Sciences and Engineering  
5 Division, under contract number DE-AC02-05CH11231 within the Inorganic/Organic  
6 Nanocomposites Program (KC3104). C. N. Eisler acknowledges support from the Office  
7 of Energy Efficiency & Renewable Energy Postdoctoral Fellowship Program (U.S.  
8 Department of Energy). We would like to thank Dr. Son Nguyen for help with  
9 synthesizing nanocrystals, and Prof. Bill Nix, Andy Minor and Raymond Jeanloz for a  
10 critical reading of the manuscript.

11

## 12 **References**

- 13 [1] J. Sun, L. He, Y.-C. Lo, T. Xu, H. Bi, L. Sun, Z. Zhang, S. X. Mao, and J. Li, *Nat.*  
14 *Mater.* **13**, 1007 (2014).
- 15 [2] O. Kovalenko, C. Brandl, L. Klinger, and E. Rabkin, *Adv. Sci.* **4**, 1700159 (2017).
- 16 [3] D. Mordehai, E. Rabkin, and D. J. Srolovitz, *Phys. Rev. Lett.* **107**, 96101 (2011).
- 17 [4] R. Kositski and D. Mordehai, *Acta Mater.* **136**, 190 (2017).
- 18 [5] W. Liang, M. Zhou, and F. Ke, *Nano Lett.* **5**, 2039 (2005).
- 19 [6] J. Wang, Z. Zeng, C. R. Weinberger, Z. Zhang, T. Zhu, and S. X. Mao, *Nat. Mater.*  
20 **14**, 594 (2015).
- 21 [7] W. L. Barnes, A. Dereux, and T. W. Ebbesen, *Nature* **424**, 824 (2003).
- 22 [8] S. Lal, S. Link, and N. J. Halas, *Nat. Photonics* **1**, 641 (2007).
- 23 [9] P. V. Kamat, *J. Phys. Chem. B* **106**, 7729 (2002).



- 1 [10] J. Zeng, Q. Zhang, J. Chen, and Y. Xia, *Nano Lett.* **10**, 30 (2010).
- 2 [11] C. Sönnichsen, B. M. Reinhard, J. Liphardt, and A. P. Alivisatos, *Nat. Biotechnol.*  
3 **23**, 741 (2005).
- 4 [12] K. A. Willets and R. P. Van Duyne, *Annu. Rev. Phys. Chem.* **58**, 267 (2007).
- 5 [13] X. Huang, I. H. El-Sayed, W. Qian, and M. A. El-Sayed, *J. Am. Chem. Soc.* **128**,  
6 2115 (2006).
- 7 [14] L. R. Hirsch, R. J. Stafford, J. A. Bankson, S. R. Sershen, B. Rivera, R. E. Price, J.  
8 D. Hazle, N. J. Halas, and J. L. West, *Proc. Natl. Acad. Sci. U. S. A.* **100**, 13549  
9 (2003).
- 10 [15] X. Xia, S. Xie, M. Liu, H.-C. Peng, N. Lu, J. Wang, M. J. Kim, and Y. Xia, *Proc.*  
11 *Natl. Acad. Sci. U. S. A.* **110**, 6669 (2013).
- 12 [16] Y. Lu, J. Y. Huang, C. Wang, S. Sun, and J. Lou, *Nat. Nanotechnol.* **5**, 218 (2010).
- 13 [17] S. Y. Kim, I.-H. Lee, and S. Jun, *Phys. Rev. B* **76**, 245407 (2007).
- 14 [18] S. H. Tolbert and A. P. Alivisatos, *Science* **265**, 373 (1994).
- 15 [19] C. L. Choi, K. J. Koski, S. Sivasankar, and A. P. Alivisatos, *Nano Lett.* **9**, 3544  
16 (2009).
- 17 [20] Q. F. Gu, G. Krauss, W. Steurer, F. Gramm, and A. Cervellino, *Phys. Rev. Lett.*  
18 **100**, 45502 (2008).
- 19 [21] Y. Bao, B. Zhao, D. Hou, J. Liu, F. Wang, X. Wang, and T. Cui, *J. Appl. Phys.*  
20 **115**, 223503 (2014).
- 21 [22] Y. Bao, B. Zhao, X. Tang, D. Hou, J. Cai, S. Tang, J. Liu, F. Wang, and T. Cui,  
22 *Appl. Phys. Lett.* **107**, 201909 (2015).
- 23 [23] A. Lay, D. S. Wang, M. D. Wisser, R. D. Mehlenbacher, Y. Lin, M. B. Goodman,

- 1 W. L. Mao, and J. A. Dionne, *Nano Lett.* **17**, 4172 (2017).
- 2 [24] K. Lance Kelly, Eduardo Coronado, A. Lin Lin Zhao, and G. C. Schatz\*, (2002).
- 3 [25] S. Link and M. A. El-Sayed, *J. Phys. Chem. B* **103**, 8410 (1999).
- 4 [26] G. V Hartland, *Chem. Rev.* **111**, 3858 (2011).
- 5 [27] N. Goubet, C. Yan, D. Polli, H. Portalès, I. Arfaoui, G. Cerullo, and M.-P. Pileni,  
6 *Nano Lett.* **13**, 504 (2013).
- 7 [28] Tanvi, A. Mahajan, R. K. Bedi, S. Kumar, V. Saxena, and D. K. Aswal, *J. Appl.*  
8 *Phys.* **117**, 83111 (2015).
- 9 [29] S. Peng, Y. Lee, C. Wang, H. Yin, S. Dai, and S. Sun, *Nano Res.* **1**, 229 (2008).
- 10 [30] C. . Herbst, R. . Cook, and H. . King, *J. Non. Cryst. Solids* **172–174**, 265 (1994).
- 11 [31] T. S. Duffy, G. Shen, D. L. Heinz, J. Shu, Y. Ma, H.-K. Mao, R. J. Hemley, and A.  
12 K. Singh, *Phys. Rev. B* **60**, 15063 (1999).
- 13 [32] A. K. Singh, H.-P. Liermann, Y. Akahama, S. K. Saxena, and E. Menéndez-  
14 Proupin, *J. Appl. Phys.* **103**, 63524 (2008).
- 15 [33] A. K. Singh, H. P. Liermann, S. K. Saxena, H. K. Mao, and S. U. Devi, *J. Phys.*  
16 *Condens. Matter* **18**, S969 (2006).
- 17 [34] C. B. Murray, C. R. Kagan, and M. G. Bawendi, *Annu. Rev. Mater. Sci.* **30**, 545  
18 (2000).
- 19 [35] M. P. Pileni, *J. Phys. Chem. B* **105**, 3358 (2001).
- 20 [36] Francois Cardarelli, *Materials Handbook* (Springer London, London, 2008).
- 21 [37] X. Qian and H. S. Park, *J. Mech. Phys. Solids* **58**, 330 (2010).
- 22 [38] C. Voisin, D. Christofilos, P. A. Loukakos, N. Del Fatti, F. Vallée, J. Lermé, M.  
23 Gaudry, E. Cottancin, M. Pellarin, and M. Broyer, *Phys. Rev. B* **69**, 195416

1 (2004).

2 [39] E. Hao, S. Li, R. C. Bailey, S. Zou, G. C. Schatz, and J. T. Hupp, *J. Phys. Chem. B*

3 **108**, 1224 (2004).

4 [40] X. Ben, P. Cao, and H. S. Park, *J. Phys. Chem. C* **117**, 13738 (2013).

5 [41] D. I. Yakubovsky, A. V. Arsenin, Y. V. Stebunov, D. Y. Fedyanin, and V. S.

6 Volkov, *Opt. Express* **25**, 25574 (2017).

7 [42] R. J. Hemley, H. Mao, G. Shen, J. Badro, P. Gillet, M. Hanfland, and D.

8 Häusermann, *Science* (80-. ). **276**, 1242 (1997).

9 [43] C. L. Choi, K. J. Koski, A. C. K. Olson, and A. P. Alivisatos, *Proc. Natl. Acad.*

10 *Sci. U. S. A.* **107**, 21306 (2010).

11 [44] A. Stevenson, A. Jones, and S. Raghavan, *Nano Lett.* **11**, 3274 (2011).

12 [45] X. Jin, M. Götz, S. Wille, Y. K. Mishra, R. Adelung, and C. Zollfrank, *Adv.*

13 *Mater.* **25**, 1342 (2013).

14 [46] See Supplementary Material [url], which includes Refs. [47-53]

15 [47] H. K. Mao, J. Xu, and P. M. Bell, *J. Geophys. Res.* **91**, 4673 (1986).

16 [48] J. Van Straaten, R. J. Wijngaarden, and I. F. Silvera, *Phys. Rev. Lett.* **48**, 97

17 (1982).

18 [49] J. Van Straaten and I. F. Silvera, *Phys. Rev. B* **37**, 6478 (1988).

19 [50] L. B. Scaffardi and J. O. Tocho, *Nanotechnology* **17**, 1309 (2006).

20 [51] E. A. Coronado and G. C. Schatz, *J. Chem. Phys.* **119**, 3926 (2003).

21 [52] U. Kreibig, *Zeitschrift Fur Phys. B* **31**, 39 (1978).

22 [53] U. Kreibig and L. Genzel, *Surf. Sci.* **156**, 678 (1985).

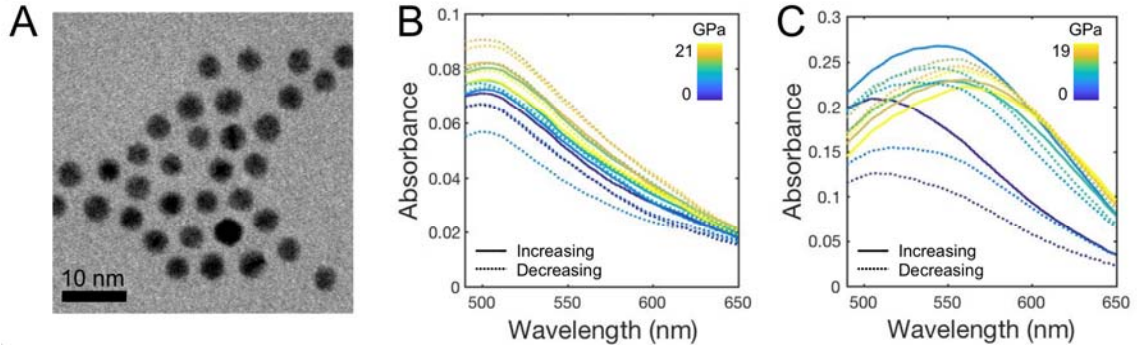
23

24

25

1 **Figures**

2



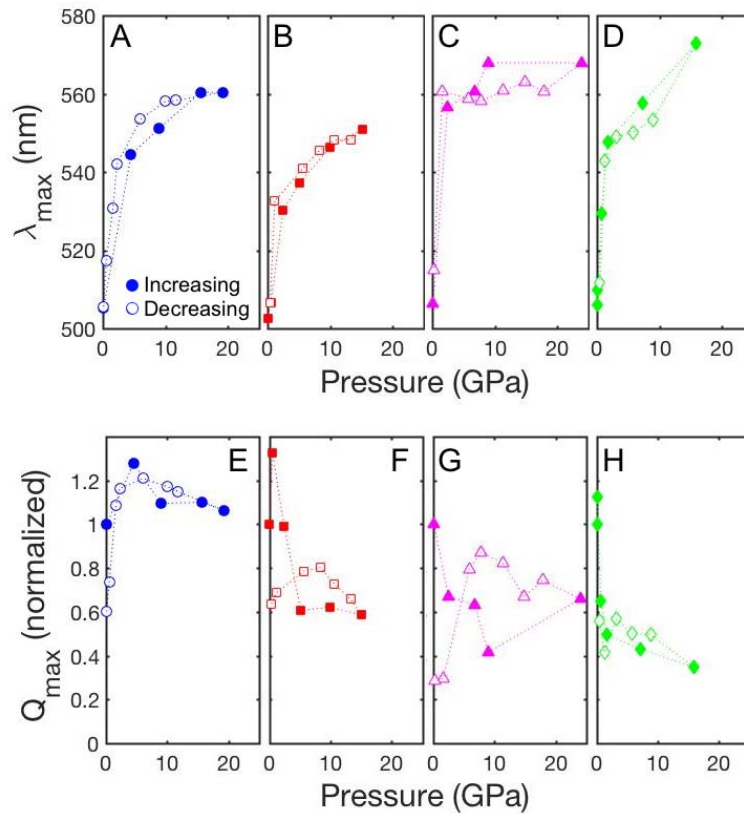
3

4

5 Figure 1. High-pressure optical absorbance. A) TEM image of 3.9 nm Au nanocrystals.  
6 Absorbance spectra in B) hydrostatic pressure medium (ethylcyclohexane) C) and non-  
7 hydrostatic pressure medium (toluene). Increasing pressures are solid lines, and  
8 decreasing pressures are dotted lines.

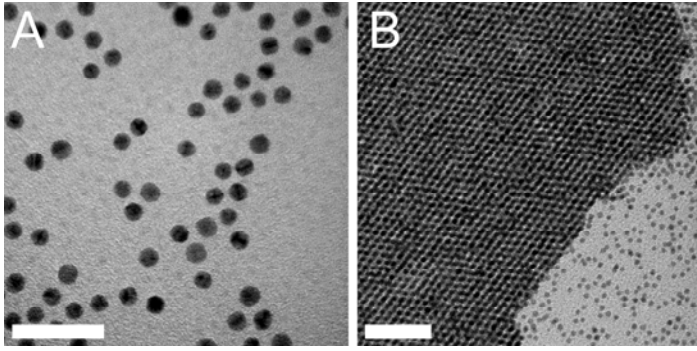
9

10



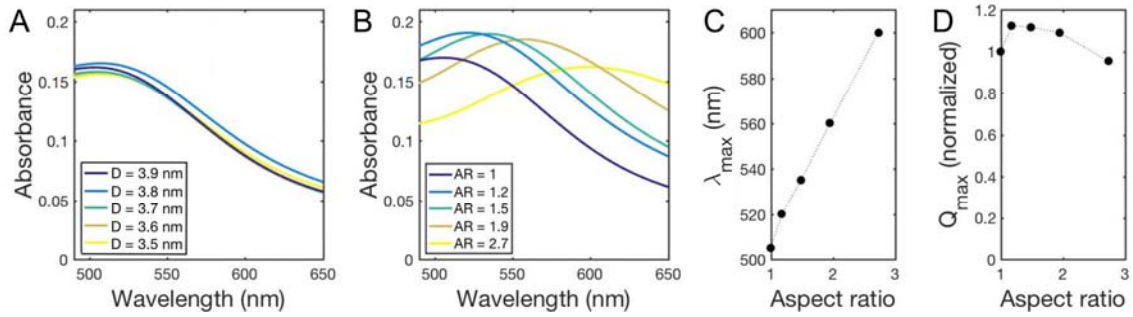
1  
 2 Figure 2. Plasmon peak shifts in a non-hydrostatic pressure environment. A-D) The  
 3 plasmon peak wavelength ( $\lambda_{\max}$ ) and E-H) the corresponding absorbance efficiency  
 4 ( $Q_{\max}$ ) for four independent experiments.  $Q_{\max}$  is normalized to  $Q_{\max}$  at ambient pressure.  
 5 Increasing pressures are filled symbols, and decreasing pressures are open symbols.

6  
7



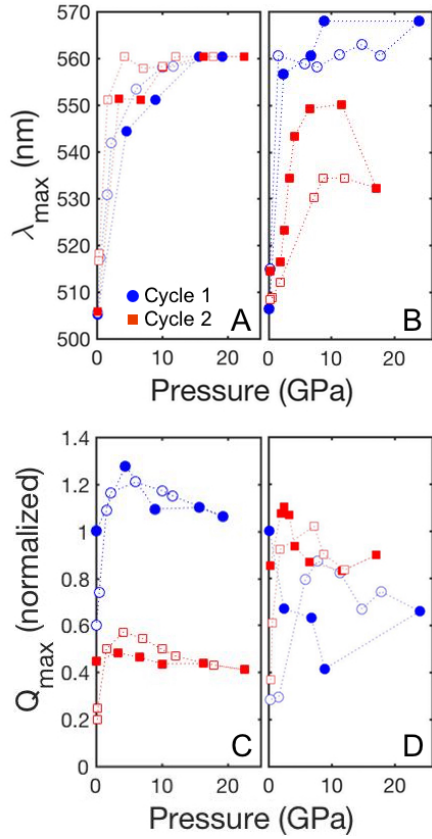
1  
2  
3  
4  
5  
6  
7

Figure 3. TEM images of A) individual (scale bar is 20 nm) and B) self-assembled superlattice of Au nanocrystals after non-hydrostatic compression to 30 GPa (scale bar is 50 nm).



1  
2  
3  
4  
5  
6  
7  
8  
9

Figure 4. Simulated optical absorbance. A) Absorbance of spherical nanocrystals with varying diameter (D). B) Absorbance of ellipsoidal spheroid nanocrystal with constant volume (equal to sphere with 3.9 nm diameter) and varying aspect ratio (AR). C) Plasmon peak wavelength ( $\lambda_{\max}$ ) and D) absorbance efficiency ( $Q_{\max}$ ) corresponding to (B).



1  
2  
3  
4  
5  
6  
7  
8

Figure 5. Multiple non-hydrostatic pressure cycles. A,B) The plasmon peak wavelength ( $\lambda_{\max}$ ) and C,D) the corresponding absorbance efficiency ( $Q_{\max}$ ) during cycle 1 (blue) and cycle 2 (red) during two experiments where the cycles are spaced apart by a half-hour (A,C), and 15.5 hours (B,D). Increasing pressures are filled symbols, and decreasing pressures are open symbols.